





Working Progress towards Lawn Mower Automation

Alfredo Chávez Plascencia¹^a, Vítězslav Beran¹^b, Jaroslav Rozman¹^c
and Aguilar Acosta Armando²^d

¹*BUT FIT IT4Innovations, Czech Republic*

²*University of Guadalajara, School of Mechatronics,
Carretera Guadalajara - Ameca Km. 45.5, C.P. 46600, Ameca, Jalisco, Mexico*

Keywords: Mobile Robot, Nonlinear Control, Path Planning.

Abstract: This paper is a working progress towards an automation of the Spider lawn mower (SLM) which is a four synchronized steering wheel mobile robot. During the functioning, the SML must follow cutting grass edge with no overlapping of a strip of cut grass and also satisfy slippage constrains. To this end, a small prototype called Andromina which is a four-independent steering wheel mobile robot has been chosen to verify the control approach. This paper proposes to implement a mathematical model that takes into account the kinematics and dynamics of the mobile robot and also a nonlinear control strategy like the state feedback linearization. The most important advantage of the proposed model-control strategy is that it takes into account the nonlinearities of the system and a control law becomes a linear one. The path following tracking error has been verified by the statistical approach called analysis t-test and also results of real data simulations have shown the effectiveness of the proposed control strategy applied to a four-independent steering nonholonomic wheeled mobile robot.


1 INTRODUCTION


Mobility and controllability of lawn mower machines (LMM) is still an immature open research field (Wasif, 2011). A brief review of the state of the art of LMM is carried out in (Wasif, 2011) where it states that (Smith et al., 2005) proposes a design of a mobile robot which lacks to discuss propositions of mowing operation. Moreover, static localization and dynamic obstacle avoidance are overlooked. And, the system is controlled manually lacking artificial intelligence. (Bing-Min and Chun-Liang, 2008) suggests an optimal route planning of a mobile robot where it does not converge autonomously to the path. Moreover, obstacle avoidance algorithm would work for static obstacles not for dynamic ones. The fundamental idea of LMM as a mobile robot is discussed in (Taj and Timothy, 2008) lacking simulation and implementation results. The work done in (Wasif, 2011) suggests a motor schema architecture to control a LMM and also the system suffers from slippage conditions. From


our point of view, the systems mentioned previously lack a complete mathematical formulation of a LMM that can potentially allow the system to be controlled by some classical control strategies. They also lack slippage uncertainties than can be added to the mathematical model of the system. The objective of this proposal is to cope with some of the drawbacks presented in the previous works by adding a mathematical model and a control functionality to the system.


To this end, some control strategies for mobile robots are found in the literature. For instance, (Mathieu et al., 2017) uses a backstepping method to address a four-wheel steering mobile robot following a path which an observer is used to estimate the lateral sliding. (Krzysztof and Dariusz, 2004) also uses a backstepping approach to solve the control issue and the stability is proof by the Lyapunov technique. (Paulo and Urbano, 2005) shows an input-output feedback-linearization method in discrete mode for the path following of wheeled mobile robots (WMRs) subject to nonholonomic constraints. (Harwood, 2016) controls a automower 330x using feedback linearization and with the feedback gain estimated using an LQ-controller.

The control strategy proposed in this article is feedback linearization which is one of the most com-

^a  <https://orcid.org/0000-0002-7505-5570>

^b  <https://orcid.org/0000-0002-7495-6932>

^c  <https://orcid.org/0000-0001-8443-433X>

^d  <https://orcid.org/0000-0003-4920-527X>

mon approaches to control nonlinear systems. The advantage of this technique is the transformation of the nonlinear system into a linear one by means of a proper transformation of variables. The intention is to apply the control strategy to the SLM and due to the Spider system is not available at the moment of this work, the system Andromina has been taken into account to apply the model-control strategy. The Spider (Spider, 2015) as well as the Andromina (Andromina, 2016b) mobile robots are shown in Figures 1 and 2 respectively.

2 METHODS

Robot operating system (ROS) (Quigley et al., 2009) is suggested to be used to handle the automation of the SLM. The navigation stack (NS) that comes with ROS installation is a set of configurable nodes that need to be set up properly to the dynamics of the mobile robot in turn. In other words, the move base node is the core of the navigation stack which offers interfaces between sensors and algorithms for: localization, local and global path planners, local and global maps. For instance, the global map is formed by the gmapping node, which is based on simultaneous localization and mapping (SLAM). Then, during the working of the robot, the NS interacts with sensor readings, localization, path planning and map algorithms to avoid obstacles on the path in order to reach a specified goal (Fox et al., 1999). Further on, the dynamic window approach planner (DWAP) and the Dijkstra's algorithm nodes are used by the NS to guarantee obstacle avoidance (Fox et al., 1997). Thus, given a global path to follow the NS uses the costmap node that takes in the sensor data to build and inflate a local 2D occupancy grid map. This package also provides support to the DWAP that generates the velocity commands that drive the robot from an initial to a final coordinate. In this approach, a nonlinear control node has been created and inserted into the NS.

3 MATHEMATICAL MODEL AND CONTROL

A four-independent steering wheeled mobile robot model and nomenclature has been inspired from (Chávez Plascencia and Dremstrup, 2011) and presented in Figure 3.

3.1 Kinematic Model

(Guy et al., 1996) imposes two restrictions to the kinematic model; *a*) Rolling without slipping and *b*) no sidelong motion. Equations 1 and 2 are the restrictions to the wheels with respect to P_c and, they can also be arranged in a more compact form as shown in Equations 3 and 4.

$$[\cos(\beta_i) \quad \sin(\beta_i) \quad l_i \sin(\beta_i - \alpha_i)] R(\theta) \dot{\xi} - r \dot{\psi}_i = 0 \quad (1)$$

$$[\sin(\beta_i) \quad -\cos(\beta_i) \quad -l_i \cos(\alpha_i - \beta_i)] R(\theta) \dot{\xi} = 0 \quad (2)$$

$$J_1(\beta_i) R(\theta) \dot{\xi} - J_2 \dot{\psi}_i = 0 \quad (3)$$

$$C_1(\beta_i) R(\theta) \dot{\xi} = 0 \quad (4)$$

where; $i = 1, 2, 3, 4$, $R(\theta)$ is the 2D rotation matrix from frame $\{E\}$ to frame $\{W\}$, $\xi = [x_c, y_c, \theta]^T$ represents the robot pose at the point P_c , $\beta_i = [\beta_1, \beta_2, \beta_3, \beta_4]^T$ is the steering wheel angle vector and $\psi_i = [\psi_1, \psi_2, \psi_3, \psi_4]^T$ is the rotation wheel angle vector. (N.Sarkar and R.V.Kumar, 1992) defines q as n generalized coordinates that fall into m restrictions which can be organized as $C(q, \dot{q})$, where k represents holonomic restrictions and $m - k$ represents nonholonomic restrictions as presented in Equation 5.

$$A(q) \dot{q} = 0 \quad (5)$$

With

$$A(q) = \begin{bmatrix} J_1(\beta) R(\theta) & 0 & -J_2 \\ C_1(\beta) R(\theta) & 0 & 0 \end{bmatrix} \quad (6)$$

$$\dot{q} = [\dot{x}_c \quad \dot{y}_c \quad \dot{\theta} \quad \dot{\beta}_i \quad \dot{\psi}_i] \quad (7)$$

where; $A(q)$ is a $(m \times n)$ full rank matrix.

Some remarks about $C(q, \dot{q})$ can be stated as follows:

- If a restriction equation is in the form $C(\dot{q})$ and it can be integrated, such restriction is a holonomic one.
- If a restriction equation is in the form $C(q)$ and it can not be integrated, such restriction is a nonholonomic one.

According to (Coelho and Nunes, 2003), the Equation $C_1(q)S(q) = 0$ can be obtained from Equation 5, where $S(q)$ is a linear independent vector field and $N(C)$ is the null space of $C_1(q)$. And, it is also possible to define a velocity $\eta(t)$ such that for all t , then Equation 8 can be stated.



Figure 1: The Spider lawn mower robot.

$$\dot{q} = S(q)\eta(t) \quad (8)$$

Equation 8 gives a kinematic model.

In order to relate Equation 8 with the four-independent steering wheeled kinematic model, the no lateral movement constraint 4 is taken. It can be seen that $R(\theta)\dot{\xi}$ lies in the null space of $\mathcal{N}(C_1(\beta))$. Then, defining $\mathcal{N}(C_1(\beta)) = \Sigma(\beta)$ yields the following relation $\mathcal{N}(C_1(\beta))\eta(t) = \Sigma(t)\eta(t) = R(\theta)\dot{\xi}$. Afterwards, isolating $\dot{\xi}$ from the previous equation and then substituting it into Equation 3 and defining the steering velocity vector $\beta = \zeta = [\zeta_1, \zeta_2, \zeta_3, \zeta_4]$, the kinematic model is obtained as shown in Equation 9 which is of the form $\dot{q} = S(q)u(t)$.

$$\dot{\xi} = [R^T(\theta)\Sigma(\theta)]\eta(t) \quad (9)$$

According to (Guy et al., 1996), in order to guarantee maneuverability δ_M of the SLM the degree of mobility δ_m and the degree of steerability δ_s , Equations 10 and 11 must satisfy the following conditions: $1 \leq \delta_m \leq 3$ and $0 \leq \delta_s \leq 2$.

$$\delta_m = \dim \mathcal{N}[C_1(\beta)] = 3 - \text{rank}[C_1(\beta)] \quad (10)$$

$$\delta_s = \text{rank}[C_1(\beta)] \quad (11)$$

3.2 Dynamic Model

The relation between the torques τ derived by the embarked motors and the change in velocities \dot{u} in the SLM can be described by the dynamic model. The equations of motion that relates τ and \dot{u} can be derived by means of the Lagrangian formalism as stated in Equation 12, (Bloch, 2000; Symon, 1971; Goldstain, 1980).

$$\begin{aligned} \frac{d}{dt} \left(\frac{\partial L(q, \dot{q})}{\partial \dot{q}} \right) - \frac{\partial L(q, \dot{q})}{\partial q} &= M_I(q)\ddot{q} + V(q, \dot{q}) \\ &= A^T(q)\lambda + B(q)\tau \end{aligned} \quad (12)$$



Figure 2: Andromina.

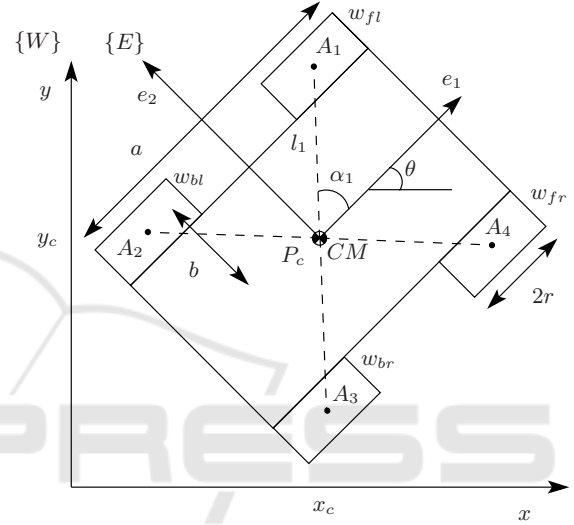


Figure 3: The four-independent steering wheeled mobile robot geometry. E is a fixed frame on the robot with axis e_1 and e_2 , W is world frame. θ is the angle of rotation, CM is the center of mass.

The definition of the nomenclature in Equation 12 is taken from (Chávez Plascencia and Dremstrup, 2011) and stated as follows:

$L(q, \dot{q})$ is called the Lagrangian.

$M_I \in \mathbb{R}^{n \times n}$ is the matrix that represents the inertia of the system.

$V(q, \dot{q}) \in \mathbb{R}^{n \times n}$ is the matrix of Coriolis.

$A(q)$ is the matrix that represents the Jacobean.

$B(q) \in \mathbb{R}^{n \times (n-m)}$ is an input transformation matrix.

$\tau \in \mathbb{R}^{(n-m)}$ is a torque vector that represents the input.

$\lambda \in \mathbb{R}^m$ is the Lagrangian multipliers.

q represents the generalized coordinates.

(Chávez Plascencia and Dremstrup, 2011) takes the potential energy of the system as constant and it is neglected from the Lagrangian multiplier. This fact leads the Lagrangian L as function of the kinetic energy T , i.e. $L = f(T)$.

To solve Equation 12, the same methodology as stated in (Chávez Plascencia and Dremstrup, 2011) is applied. This is done in three steps. First, an individual kinetic energy of each wheel is solved. Second, the kinetic energy of the chassis is also solved. And, finally, all the energies are added to get a single energy.

The kinetic energy T_w of a single steering wheel attached to the trolley can be obtained by integration of an infinitesimal mass $d_m[Kg]$ of a point $P_w(x_{P_w}, y_{P_w}, z_{P_w})$ which is placed on the surface of the wheel. The radius r from the center of the wheel to the point P_w forms an angle ψ . Then, the velocity of the point P_w on the wheel is solved and then multiplied by the angular density $\rho_\alpha[Kg/rad]$. The former process is shown in Equations 13 and 14.

$$P_w = \begin{bmatrix} x_c + l\cos(\alpha + \theta) + r\cos(\psi)\cos(\theta + \beta) \\ y_c + l\sin(\alpha + \theta) + r\cos(\psi)\sin(\theta + \beta) \\ r\sin(\psi) \end{bmatrix} \quad (13)$$

$$T_w = \frac{1}{2} \int_0^{2\pi} (\dot{x}_{P_w}^2 + \dot{y}_{P_w}^2 + \dot{z}_{P_w}^2) \rho_\alpha d\psi \quad (14)$$

The kinetic energy of each individual wheel can be obtained by inserting Equation 13 into Equation 14. The result is shown in Equation 15.

$$T_w = \frac{1}{2} m_w \dot{x}_c^2 + \frac{1}{2} m_w \dot{y}_c^2 + m_w l \dot{\theta} (\dot{y}_c \cos(\alpha + \theta) - \dot{x}_c \sin(\alpha + \theta)) + \frac{1}{2} m_w l^2 \dot{\theta}^2 + \frac{1}{2} I_w \dot{\psi}^2 + \frac{1}{4} I_w \dot{\beta}^2 + \frac{1}{2} I_w \dot{\theta} \dot{\beta} + \frac{1}{4} I_w \dot{\theta}^2 \quad (15)$$

$I_w = m_w r^2$ being the wheel's inertia and $m_w = 2\pi\rho_\alpha$ the mass' wheel.

(Chávez Plascencia and Dremstrup, 2011) states that the kinetic energy of a moving chassis can be obtained by adding translational and rotational energies, as it is presented in Equation 16.

$$T_F = \frac{1}{2} M_T (\dot{x}_c^2 + \dot{y}_c^2) + \frac{1}{2} I_T \dot{\theta}^2 \quad (16)$$

$$\dot{x}_c = \dot{x} - d\dot{\theta}\sin(\theta + \rho) \quad (17)$$

$$\dot{y}_c = \dot{y} + d\dot{\theta}\cos(\theta + \rho) \quad (18)$$

Where; $M_T[Kg]$ is the chassis's mass, $(\dot{x}_c^2 + \dot{y}_c^2)[m/sec]$ is the linear velocity of the trolley about its CM , $I_T[Kg \cdot m^2]$ is the inertia's moment of the chassis,

$\dot{\theta}[Rad/s]$ is the angular velocity and $d[m]$ is the distance from the CM to the center of the robot.

Then, inserting 17 and 18 into 16, the Equation 19 is obtained. This equation represents the kinetic energy of the chassis of the robot.

$$T_F = \frac{1}{2} M_T \dot{x}_c^2 + \frac{1}{2} M_T \dot{y}_c^2 + \frac{1}{2} M_T d^2 \dot{\theta}^2 + \frac{1}{2} I_T \dot{\theta}^2 - M_T d \dot{x}_c^2 \dot{\theta} \sin(\theta + \rho) + M_T d \dot{y}_c^2 \dot{\theta} \cos(\theta + \rho) \quad (19)$$

By adding the individual wheel kinetic energy with the chassis kinetic energy a total kinetic energy is obtained as it can be seen in Equation 20.

$$T = T_F + \sum_{i=1}^4 T_{w_i} \quad (20)$$

By expanding Equation 20 and then arranging it into a matrix form gives Equation 21 which is the total kinetic energy of the SLM with respect to its CM .

$$T = \frac{1}{2} \dot{\xi}^T R(\theta)^T M R(\theta) \dot{\xi} + \frac{1}{4} \dot{\beta}^T I_{WM} \dot{\beta} + \frac{1}{2} \dot{\psi}^T I_{WM} \dot{\psi} + \frac{1}{2} \dot{\theta} I_{WV} \dot{\beta} \quad (21)$$

Where :

$$I_{WM} = \begin{bmatrix} I_w & 0 & 0 & 0 \\ 0 & I_w & 0 & 0 \\ 0 & 0 & I_w & 0 \\ 0 & 0 & 0 & I_w \end{bmatrix}$$

$$I_{WV} = \begin{bmatrix} I_w & I_w & I_w & I_w \end{bmatrix}$$

$$M = \begin{bmatrix} M_1 & 0 & M_2 \\ 0 & M_1 & M_3 \\ 0 & 0 & M_4 \end{bmatrix}$$

$$M_1 = M_T + 4m_w$$

$$M_2 = -2 \left[d M_T \sin(\rho) + m_w \sum_{i=1}^4 l_i \sin(\alpha_i) \right]$$

$$M_3 = 2 \left[d M_T \cos(\rho) + m_w \sum_{i=1}^4 l_i \cos(\alpha_i) \right]$$

$$M_4 = d^2 M_T + I_T + m_w \sum_{i=1}^4 l_i^2 + 2I_w \quad (22)$$

The dynamic model of the SLM with emphasis in steering wheels can be derived according to the procedure stated in (Guy et al., 1996). To this end, the matrices $A^T(q)$ and $B(q) = [0_{3 \times 8}; \mathbb{I}_{8 \times 8}]$ are replaced in the right expression of Equation 12. The Lagrange equations of motion of the SLM with Lagrangian multipliers λ_1 and λ_2 are given by Equations 23 to 25.

$$\frac{d}{dt} \left(\frac{\partial T}{\partial \dot{\xi}} \right) - \frac{\partial T}{\partial \xi} = [T]_{\xi} = R^T(\theta) J_1^T(\beta) \lambda_1 + R^T(\theta) C_1^T(\beta) \lambda_2 \quad (23)$$

$$\frac{d}{dt} \left(\frac{\partial T}{\partial \dot{\beta}} \right) - \frac{\partial T}{\partial \beta} = [T]_{\beta} = \tau_{\beta} \quad (24)$$

$$\frac{d}{dt} \left(\frac{\partial T}{\partial \dot{\psi}} \right) - \frac{\partial T}{\partial \psi} = [T]_{\psi} = -J_2^T \lambda_1 + \tau_{\psi} \quad (25)$$

The next step is to eliminate the Lagrange coefficients from Equations 23 and 25. To do so, the Equations 23 and 25 are premultiplied from the left with $\Sigma(\beta)R(\theta)$ and $\Sigma^T(\beta)J_1^T(\beta)J_2^{-T}$ respectively, and then summed up and taking into account that $\Sigma^T(\beta)C_1^T(\beta) = 0_{1 \times 4}$. This leads to two equations, from which the Lagrange coefficients have been disappeared. Furthermore, the total kinetic energy Equation 21 is inserted in the left side of Equations 23, 24 and 25 respectively. Once $[T]_{\xi}$, $[T]_{\beta}$ and $[T]_{\psi}$ are solved, they are inserted in the first two equations with no Lagrangian coefficients. This step leads up to two new equations that contain the velocity $\dot{\xi}$, $\dot{\psi}$, $\dot{\beta}$ and acceleration $\ddot{\xi}$, $\ddot{\psi}$, $\ddot{\beta}$ terms. Then, with the aid of the kinematic equations and their derivatives and substituting them back and arranged them in a matrix format yields the Equation 26 which is the dynamic model of the system.

$$H(\beta)\dot{u} + f(\beta, u) = F(\beta)\tau \quad (26)$$

Where:

$$\begin{aligned} \tau &= \begin{bmatrix} \tau_{\psi} \\ \tau_{\beta} \end{bmatrix} \\ F(\beta) &= \begin{bmatrix} \Sigma^T(\beta)E^T(\beta) & 0_{4 \times 4} \\ 0_{4 \times 4} & I_{4 \times 4} \end{bmatrix} \\ P &= \begin{bmatrix} M_1 & 0 & P_1 \\ 0 & M_1 & P_2 \\ P_3 & P_4 & M_4 \end{bmatrix} \\ P_1 &= \frac{1}{2}(M_2 \cos(\theta) - M_3 \sin(\theta)) \\ P_2 &= \frac{1}{2}(M_3 \cos(\theta) + M_2 \sin(\theta)) \\ P_3 &= \frac{1}{2}(M_2 \cos(\theta) - M_3 \sin(\theta)) \\ P_4 &= \frac{1}{2}(M_3 \cos(\theta) + M_2 \sin(\theta)) \\ E(\beta) &= J_2^{-1} J_1(\beta) \\ f(\beta, u) &= \begin{bmatrix} f_1(\beta, u) \\ f_2(\beta, u) \end{bmatrix} \end{aligned} \quad (27)$$

$$f_1(\beta, u) = \Sigma^T(\beta) \left[R(\theta) \dot{P} R^T(\theta) + R(\theta) P \dot{R}^T(\theta) - \frac{1}{2} R(\theta) K_1 \eta^T \Sigma^T(\beta) N + E^T(\beta) I_{WM} \dot{E}(\beta) \right] \Sigma(\beta) \eta$$

$$+ \Sigma^T(\beta) \left[R(\theta) P R^T(\theta) + E^T(\beta) I_{WM} E(\beta) \right] \dot{\Sigma}(\beta) \eta$$

$$f_2(\beta, u) = \frac{1}{2} \ddot{\theta} I_w K_2$$

$$H(\beta) = \begin{bmatrix} H_1(\beta) & H_2(\beta) \\ 0_{1 \times 4} & \frac{1}{2} I_{WM} \end{bmatrix}$$

$$H_1(\beta) = \Sigma^T(\beta) \left[R(\theta) P R^T(\theta) + E^T(\beta) I_{WM} E(\beta) \right] \Sigma(\beta)$$

$$H_2(\beta) = \frac{1}{2} \Sigma^T(\beta) R(\theta) K_1 I_{wV}$$

The kinematics and dynamics of the SLM can be written in state space representation as stated in Equations 28 and 29.

$$H(\beta)\dot{u} = -f(\beta, u) + F(\beta)\tau \quad (28)$$

$$\dot{q} = S(q)u \quad (29)$$

3.3 Control by Feedback Linearization

State feedback linearization has been chosen to tackle the dynamics of the system. (Coelho and Nunes, 2003; Chávez Plascencia and Dremstrup, 2011) state that if in a nonlinear system one or more restrictions are nonholonomic the system is not fully state linearizable, however it can be input-output linearizable.

One of the characteristics in input-output feedback linearization is to find a change of variables such that $z = T(x)$ and $x = T^{-1}(z)$ is diffeomorphism, bringing the nonlinear system into a normal form. This form decomposes the nonlinear system into external and internal parts respectively, making the system partially linearizable. The output of the system in turn can see the external variables but not the internal ones. The external part can be linearized and be transformed into a linear canonical form. It would be worth to analyzing the stability of the internal part by means of the zero dynamics of the system (Khalil, 2002; Marquez, 2003). When dealing with the external part, the number of output equations can be chosen by means of the relative degree of the system.

To this end, the state representation stated in Equations 28 and 29 is arranged in the following matrix form.

$$\begin{bmatrix} \dot{q} \\ \dot{u} \end{bmatrix} = \begin{bmatrix} S(q)u \\ -H^{-1}f \end{bmatrix} + \begin{bmatrix} 0 \\ H^{-1}f \end{bmatrix} \tau \quad (30)$$

In the previous matrix expression, u is defined as $[\eta, \beta_1, \beta_2]$. Notwithstanding, the angular velocities $[\dot{\beta}_1, \dot{\beta}_2]$ are not taken into account because \dot{q} depends only on η then $u = \eta$.

The state representation stated in Equation 30 can be linearized by choosing a nonlinear feedback Equation $\tau = F^\dagger[Hv + f]$ and it can also be arranged in a general nonlinear form as shown in Equations 31, 32 and 33.

$$\begin{aligned} \dot{x} &= f(x) + g(x)\eta \\ y &= h(x) \end{aligned} \quad (31)$$

$$\begin{aligned} \begin{bmatrix} \dot{q} \\ \dot{\eta} \end{bmatrix} &= \begin{bmatrix} S(q)\eta \\ 0 \end{bmatrix} + \begin{bmatrix} 0 \\ 1 \end{bmatrix} v \\ y &= h(q) \end{aligned} \quad (32)$$

$$\dot{x} = \begin{bmatrix} \dot{q} \\ \dot{\eta} \end{bmatrix}, f(x) = \begin{bmatrix} S(q)\eta \\ 0 \end{bmatrix}, g(x) = \begin{bmatrix} 0 \\ 1 \end{bmatrix} \quad (33)$$

In order to achieve input-output linearization, an analysis of the output equation $y = h(q)$ must be taken. In other words, the position vector $q = [x_c, y_c, \theta]$ is of interest, then three output equations are formulated as stated in the Equation 34.

$$h(q) = \begin{bmatrix} h_1(q) \\ h_2(q) \\ h_3(q) \end{bmatrix} = y = \begin{bmatrix} y_1 \\ y_2 \\ y_3 \end{bmatrix} = \begin{bmatrix} x_c \\ y_c \\ \theta \end{bmatrix} \quad (34)$$

The output Equation 34 must be derived till it finds the input $\dot{\eta}$ (Khalil, 2002). Equation 35 shows that the output y has been derived twice till it finds the input $\dot{\eta}$, thus having a relative degree $\rho_r = 2$.

$$\begin{aligned} \dot{y} &= Jh(q)S(q)\eta \\ \ddot{y} &= \dot{\Phi}(q)\eta + \Phi(q) \end{aligned} \quad (35)$$

Where:

$$J = \begin{bmatrix} \frac{\partial q}{\partial x_c} \\ \frac{\partial q}{\partial y_c} \\ \frac{\partial q}{\partial \theta} \end{bmatrix}, \Phi(q) = Jh(q)S(q) \quad (36)$$

J is the Jacobean. Since $\dot{q} = \dot{\xi} = R^T(\theta)\Sigma(\beta)\eta$ Equation 35 can also be arranged as follows:

$$\begin{aligned} \dot{y} &= R^T(\theta)\Sigma(\beta)\eta \\ \ddot{y} &= \dot{R}^T(\theta)\Sigma(\beta)\eta + R^T(\theta)\dot{\Sigma}(\beta)\eta + R^T(\theta)\Sigma(\beta)\dot{\eta} \end{aligned} \quad (37)$$

A state variable transformation vector which is a diffeomorphism as defined in (Andersen et al., 2002) is stated as follows.

$$\begin{aligned} z &= T(q) = [z_{1:6}]^T = [y_{1:3}, \dot{y}_{1:3}]^T = \begin{bmatrix} y \\ \dot{y} \end{bmatrix} \\ &= \begin{bmatrix} h(q) \\ L_f h(q) \end{bmatrix} = \begin{bmatrix} h(q) \\ R^T(\theta)\Sigma(\beta)\eta \end{bmatrix} \end{aligned} \quad (38)$$

The system under the new state variable transformation vector $T(q)$ is characterized by the following dynamics:

$$\begin{aligned} \dot{z} &= [\dot{z}_{1:6}]^T = \begin{bmatrix} \dot{y} \\ \ddot{y} \end{bmatrix} = \begin{bmatrix} \dot{\xi} \\ \frac{d}{dt}(R^T(\theta)\Sigma(\beta)\eta) \end{bmatrix} \\ &= A_c z + B_c \beta(z)[v - \alpha(z)] \end{aligned} \quad (39)$$

Where:

$$A_c = \begin{bmatrix} 0_{3 \times 3} & \mathbb{I}_{3 \times 3} \\ 0_{3 \times 3} & 0_{3 \times 3} \end{bmatrix}, B_c = \begin{bmatrix} 0_{3 \times 3} \\ \mathbb{I}_{3 \times 3} \end{bmatrix} \quad (40)$$

$\beta(z)$ and $\alpha(z)$ are found by calculating $\frac{d}{dt}(R^T(\theta)\Sigma(\beta)\eta)$ as it is shown as follows:

$$\beta(z)[v - \alpha(z)] = \frac{d}{dt}(R^T \Sigma(\theta) \eta)$$

Where :

$$\begin{aligned} \beta(z) &= R^T(\theta) [\Sigma(\beta) \ S_g \eta] \\ \alpha(z) &= -\beta^{-1}(z) \dot{R}^T(\theta) \Sigma(\theta) \eta \\ \hat{v} &= [\dot{\eta} \ \zeta_1 \ \zeta_2] \end{aligned}$$

$$S_g = \begin{bmatrix} (s_{11} + s_{12}) & (s_{13} + s_{14}) \\ (s_{21} + s_{22}) & (s_{23} + s_{24}) \\ (s_{31}) & (s_{32}) \end{bmatrix}$$

With :

$$\begin{aligned} s_{11} &= -l_1 \cos(\beta_2) \sin(\beta_1 - \alpha_1) \\ s_{12} &= l_2 \sin(\beta_1) \cos(\beta_2 - \alpha_2) \\ s_{13} &= -l_1 \cos(\beta_2) \cos(\beta_1 - \alpha_1) \\ s_{14} &= l_2 \cos(\beta_1) \sin(\beta_2 - \alpha_2) \\ s_{21} &= -l_1 \sin(\beta_2) \cos(\beta_1 - \alpha_1) \\ s_{22} &= -l_2 \cos(\beta_1) \cos(\beta_2 - \alpha_2) \\ s_{23} &= l_1 \cos(\beta_2) \cos(\beta_1 - \alpha_1) \\ s_{24} &= l_2 \sin(\beta_1) \sin(\beta_2 - \alpha_2) \\ s_{31} &= \cos(\beta_1 - \beta_2) \\ s_{32} &= -\cos(\beta_1 - \beta_2) \end{aligned}$$

In the previous Equations $v = [\dot{\eta} \ \zeta_1 \ \zeta_2]^T$ and $\hat{v} = [\dot{\eta} \ \zeta_1 \ \zeta_2]^T$, e.g. $v \neq \hat{v}$. This mean that the input to the

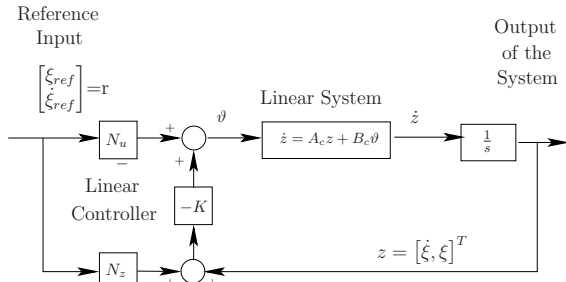


Figure 4: Shows the linear system together with the reference input.

model v given by equation 32 is not the same as the input \hat{v} given by the design control law. This problem can be solved by differentiating the last two terms of \hat{v} .

Moreover, the control law of the form $\hat{v} = \alpha(z) + \beta^{-1}(z)\vartheta$ transforms the system represented in Equation 39 into a linear one as it is shown in Equation 41.

$$\dot{z} = A_c z + B_c \vartheta \quad (41)$$

This linearized system is a controllable one. And, this can be easily verified by just looking at the matrices A_c and B_c which are in controllable canonical form. The vector ϑ which contains the accelerations from the linear controller has to be designed in order for the robot to follow a reference input r . According to the linear control theory (Franklin and Powell, 1994) the control input ϑ that allows the system to follow the reference input r is stated in Equation 42.

$$\vartheta = -Kz + (N_u + KN_z) \quad (42)$$

Where :

$$N_u = -B_c^{-1}A_c C_c^{-1}$$

$$N_x = C_c^{-1}$$

$$r = [x_c, y_c, \theta, \dot{x}_c, \dot{y}_c, \dot{\theta}]^T$$

Figure 4 shows the linearized system together with the reference control input r .

4 CONTROL SIMULATION RESULTS

The andromina ROAD-OFF V.2.0 robot (Andromina, 2016a) has been used as a test platform. It has been equipped with the following hardware; Lenovo ThinkPad L540 + Intel(R) Core(TM) i7-4712MQ CPU @ 2.30GHz, Arduino Mega 2560

(Arduino, 2016), Four Micro DC motors with encoders (SKU, 2016), Four Servos, Hokuyo URG-04LX-UG01 laser scanner (Hokuyo, 2009), Adafruit Motor/Stepper/Servo Shield for Arduino v2 Kit - v2.3 (Adafruit, 2016a), Adafruit 16-Channel 12-bit PWM/Servo Shield (Adafruit, 2016b). Figures 5 and 6 show the Andromina and the implemented hardware.

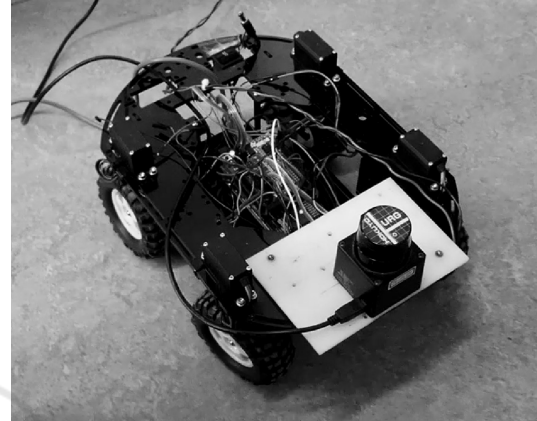


Figure 5: Shows the equipped andromina robot.

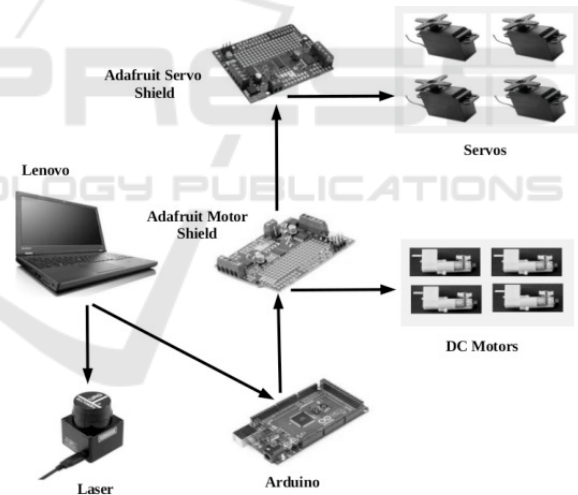


Figure 6: The Lenovo laptop communicates over a USB cables to the laser and Arduino. This in turn communicates with the Adafruit motor and servo shields which communicates with the four DC motors and four servos respectively.

The simulation has been carried out in two steps, firstly it is simulated under Octave and secondly under ROS.

4.1 Octave Simulation

A realistic path from a laboratory using a real map under ROS-RVIZ have been taken and stored in memory and then loaded with an Octave function for its anal-

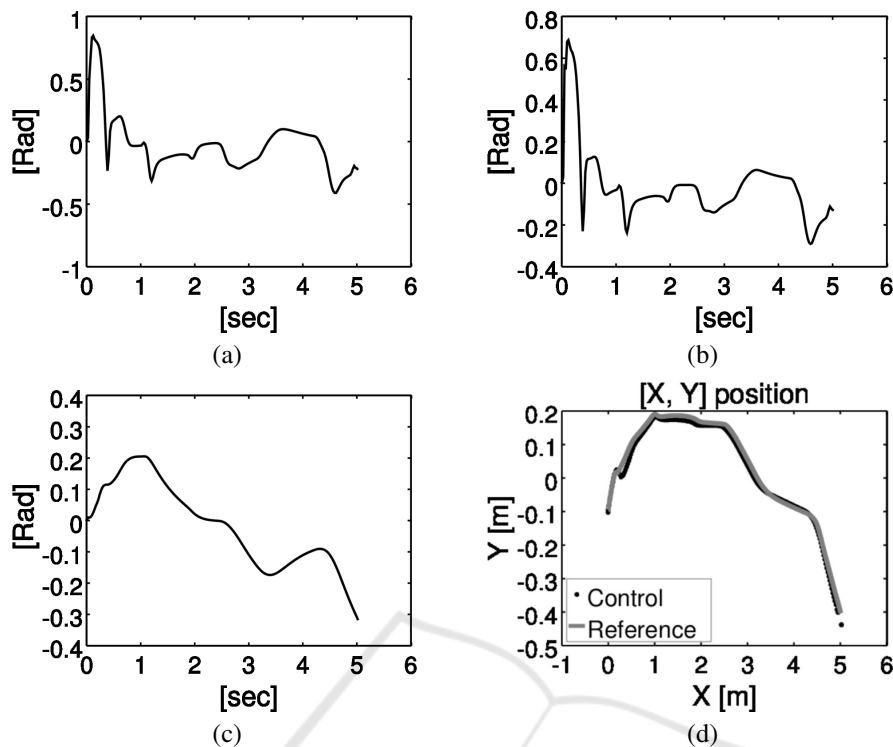


Figure 7: (a) Angle β_1 . (b) Angle β_2 . (c) Angle θ . (d) Control trajectory and the reference input.

ysis. The results of the nonlinear control simulation can be depicted in Figure 7(a-c). The angles β_1 and β_2 are shown in Figure 7(a)(b). It can be seen that these angles oscillate around 0 degrees, this means that they do not move far from the robot chassis, in other words, one can say that the nonlinear model generates the proper steering angles for the wheels to follow the trajectory path. Figure 7(c) depicts the angle θ which is the angle of the robot chassis frame with respect to the world frame. Finally, the ROS-RVIZ planned trajectory is shown in Figure 7(d) as a dark gray color whereas the nonlinear control that follows the planned trajectory is shown as a bright gray color. It can easily be noticed how the control moves the chassis $[x_c, y_c]$ according to the planned path and as mentioned earlier.

The previous parameters β_1 , β_2 , θ and the nonlinear control path tracking $[x_c, y_c]$ which are depicted in Figure 7(a-c) have been taken as the inputs of an Octave function called "*animation2(x_c, y_c, θ , β_1 , β_2)*". The outcome of the simulated result is shown in Figure 8. In this figure, the position of the robot $[x_c, y_c]$ is represented as an asterisk during the tracking path, the chassis is represented as black square which center is the position of the robot $[x_c, y_c]$, the wheels are represented as black rectangles which center is placed at each vertex of the chassis. It can be noticed that the orientation of the wheels, angles β_1 , β_2 , β_3 and β_4

correspond to the orientation of the tracking path and the perpendicular wheel lines shall meet a single ICR.

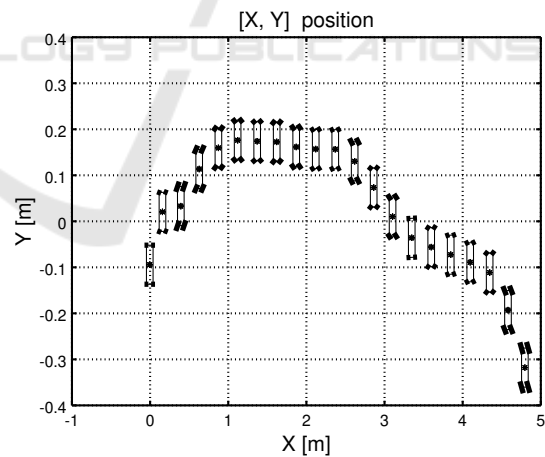


Figure 8: Shows the chassis and position of the center of gravity during the control trajectory. And, also shows the position of the wheels according to the trajectory.

4.2 ROS Simulation

The results of the created ROS node that simulates the nonlinear system can be depicted in Figures 9 and 10. At the start of the simulation, the ROS node waits for the initial position which is achieved by left mouse clicking on the "2D Pose Estimate" RVIZ but-

ton. Then, by left clicking on the "2D Nav Goal" RVIZ button a destination goal is chosen and the stable path is loaded and the control starts tracking the reference path as it is depicted in Figure 10. It can also be seen in this Figure that the laser position got shifted.

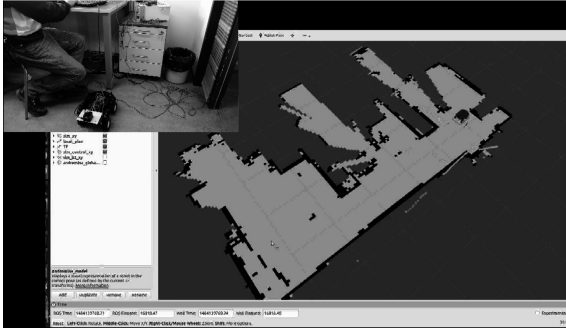


Figure 9: The Figure shows the initial position and orientation of the robot.

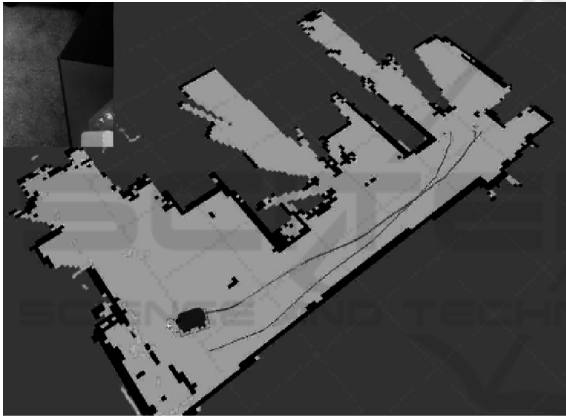


Figure 10: The darkest line is the stable loaded path and the less dark line is the tracking control. The shifted line is the tracking laser position.

4.3 Independent t-test

By looking at the Figure 7(d) one can see that two trajectories are almost identical, however it is necessary to show if there is any statistical evidences to affirm or reject this statement. To this end, differences in the two trajectories were assessed by t-test statistics. For that, two hypothesis were established: null hypothesis $H_0 : \mu_1 = \mu_2$ and alternative hypothesis $H_1 : \mu_1 \neq \mu_2$. The aim of the t-test is to accept or reject the null hypothesis. For that, two t-values are needed namely the calculated t-value and the critical t-value. If the calculated t-value is greater than the critical t-value then the null hypothesis is rejected. In order to calculate the t-value, the mean μ , variance σ^2 and sample size n of each trajectory must be obtained. The t-value can be computed by the Equation 43, whereas the criti-

cal t-value can be got from the t-table 1 which shows that the calculated t-value is less than critical t-value. Then, the null hypothesis can be accepted.

$$t = \frac{\mu_1 - \mu_2}{\sqrt{\frac{\sigma_1^2}{n_1} + \frac{\sigma_2^2}{n_2}}} \quad (43)$$

Table 1: The table shows the mean, variance of the planned trajectory as well as the control. It also shows the t-value and the t-critical.

	trajectory (n=60)		Control (n=60)	
	Mean	Variance	Mean	Variance
	0.087	0.007	0.083	0.009
t-value	0.23585			
t-critical	1.980			

5 CONCLUSION

Nonlinear control is the strategy used to solve the nonlinearities of the system. Moreover, the system turned out to be a input output linearizable and with a proper change of variables the system was transformed into a linear one. Then, linear control strategy was used for the path following. The Octave-ROS simulated results have shown that the robot follows the path and the steering angles are according to the path trajectory. Furthermore, the two trajectories were validated by the statistical t-test. In order to continue with the progress of the automation of the Spider lawn mower, the intention is to adapt the four independent steering wheel Andromina model-control to the four synchronized steering wheel Spider mobile robot. It is necessary to research further under which conditions the control is unstable or the control is robust. It is also intended to compare the current control strategy with other optimal control techniques, e.g. fuzzy control, backstepping among others.

ACKNOWLEDGMENT

This work was supported by the project IT4Innovations excellence in science, Czech Ministry of Education, Youth and Sports LQ1602 and by the project IGA FIT-S-20-6427.

REFERENCES

Adafruit (2016a). *Adafruit Motor Shield*. Available at <https://www.adafruit.com/product/1438>.

- Adafruit (2016b). *Adafruit Servo Shield*. Available at <https://www.adafruit.com/product/1411>.
- Andersen, P., Pedersen, S. T., and Dimon, J. (2002). Robust feedback linearization-based control design for a wheeled mobile robot. Proc. of the 6th International Symposium on Advanced Vehicle Control.
- Andromina (2016a). *Andromia OFF-ROAD*. Available at <http://androminarobot.blogspot.mx/p/montaje.html>.
- Andromina (2016b). *Andromina v.1.2*. Available at <http://androminarobot.blogspot.cz/search/label/Arduino>.
- Arduino (2016). *Arduino Mega 2560*. Available at <https://www.arduino.cc/en/Main/arduinoBoardMega2560>.
- Bing-Min, S. and Chun-Liang, L. (2008). Design of an autonomous lawn mower with optimal route planning. In *Industrial Technology, 2008. ICIT 2008. IEEE International Conference on*, pages 1–6, Chengdu. IEEE. ISBN: 978-1-4244-1705-6.
- Bloch, A. M. (2000). *Nonholonomic Mechanics and Control*. Addison-Wesley Publishing Company. ISBN: 0-387-95535-6.
- Chávez Plascencia, A. and Dremstrup, K. (2011). Differential mobile robot based wheelchair. Technical report, Aalborg University.
- Coelho, P. and Nunes, U. N. (2003). Lie algebra application to mobile robot control: a tutorial. *Robotica*, 21:483–493.
- Fox, D., Burgard, W., Frank, D., and Thrun, S. (1999). Monte carlo localization: Efficient position estimation for mobile robots. In *in proc. of the national conference on artificial intelligence, AAAI*, pages 343–349.
- Fox, D., Burgard, W., and Thrun, S. (1997). The dynamic window approach to collision avoidance. *Robotics & Automation Magazine, IEEE*, 4(1):23–33.
- Franklin, G. F. and Powell, J. D. (1994). *Feedback Control of Dynamic Systems, third edition*. Addison-Wesley. ISBN: 0-201-53487-8.
- Goldstain, H. (1980). *Nonholonomic Mechanics and Control*. Addison-Wesley. ISBN: 0-201-02918-9.
- Guy, C., Georges, B., and Brigitte, D. A.-n. (1996). Structural properties and classification of kinematic and dynamic models of wheeled mobile robots. *IEEE Transactions on Robotics and Automation*, pages 47–62.
- Harwood, P. (2016). Non-linear automatic control of autonomous lawn mower. Master's thesis, Linköping University, SE-581 83 Linköping, Sweden.
- Hokuyo (2009). *URG-04LX-UG01*. Available at https://www.hokuyo-aut.jp/02sensor/07scanner/urg_04lx_ug01.html.
- Khalil, H. (2002). *Nonlinear Systems*. Prentice Hall. ISBN: 0-13-067389-7.
- Krzysztof, K. and Dariusz, P. (2004). Modeling and control of a 4-wheel skid-steering mobile robot. *International Journal of Applied Mathematics Computer Science*, 14(4):477–496.
- Marquez, H. J. (2003). *Nonholonomic Control Systems Analysis and Design*. Wiley. ISBN: 0-471-42799-3.
- Mathieu, D., Roland, L., Adrian, C., Christophe, C., and Benoit, T. (2017). Path tracking of a four-wheel steering mobile robot: A robust off-road parallel steering strategy. *IEEE European Conference on Mobile Robots (ECMR)*.
- N.Sarkar, N. and R.V.Kumar (1992). Control of mechanical systems with rolling constraints: Application to dynamic control of mobile robots. Technical report, Department of Computer & Information Science (CIS), University of Pennsylvania.
- Paulo, C. and Urbano, N. (2005). Path-following control of mobile robots in presence of uncertainties. *IEEE International Journal of Transactions on Robotics*, 21(2):452–261.
- Quigley, M., Conley, K., Gerkey, B., Faust, J., Foote, T. B., Leibs, J., Wheeler, R., and Ng, A. Y. (2009). ROS: an open-source robot operating system. In *ICRA Workshop on Open Source Software*.
- SKU (2016). *DC Motor with Encoder*. Available at https://www.dfrobot.com/wiki/index.php/Micro_DC_Motor_with_Encoder-SJ02_SKU:_FIT0450.
- Smith, J., Campbell, S., and Morton, J. (2005). Design and implementation of a control algorithm for an autonomous lawnmower. In *Circuits and Systems, 2005. 48th Midwest Symposium on*, volume 1, pages 456–459, Covington, KY. IEEE. ISBN: 0-7803-9197-7.
- Spider (2015). *Mini, ILD01, ILD02*. Available at https://www.slope-mower.com/spider-ild01_p12.html.
- Symon, K. R. (1971). *Mechanics*. Addison-Wesley World student series. Addison-Wesley Publishing Company. ISBN: 9780201073928.
- Taj, B. M. and Timothy, K. T. C. (2008). Design and modelling a prototype of a robotic lawn mower. In *Information Technology, 2008. ITSIM 2008. International Symposium on*, volume 4, pages 1–5, Kuala Lumpur, Malaysia. IEEE. ISBN: 978-1-4244-2327-9.
- Wasif, M. (2011). Design and implementation of autonomous lawn-mower robot controller. In *7th International Conference on Emerging Technologies (ICET)*, pages 1–5. IEEE. ISBN: 978-1-4577-0769-8.